A GEANT4 simulation study of BESIII endcap TOF upgrade*

ZHANG Hui(张辉)[2] SHAO Ming(邵明)[1,2;1)] LI Cheng(李澄)[1,2;2)] CHEN Hong-Fang(陈宏芳)[1,2]
HENG Yue-Kun(衡月昆)[3] SUN Yong-Jie(孙勇杰)[1,2] TANG Ze-Bo(唐泽波)[1,2]
JI Chang-Sheng(姬长胜)[1,3] CHEN Tian-Xiang(陈天翔)[2] YANG Shuai(杨帅)[2]

[1] State Key Laboratory of Particle Detection and Electronics, University of Science and Technology of China, Hefei 230026, China
[2] Department of Modern Physics，University of Science and Technology of China, Hefei 230026, China
[3] Institute of High Energy Physics, Chinese Academy of Sciences, Beijing 100049, China

Abstract: A GEANT4-based Monte-Carlo (MC) model is developed to study the performance of endcap time-of-flight (ETOF) at BESIII. It's found that the multiple scattering effects, mainly from the materials at the MDC endcap, can cause multi-hit on the ETOF's readout cell and significantly influence the timing property of ETOF. A multi-gap resistive plate chamber (MRPC) with a smaller readout cell structure is more suitable for the ETOF detector due to significantly reduced multi-hit rate (per channel), from 71.5% for currently-used scintillator-based ETOF to 21.8% or 16.7% for MRPC-based ETOF, depending on the readout pad size used. The timing performance of an MRPC ETOF is also improved. These simulation results suggest and guide an ETOF upgrade effort at BESIII.

Key words: BESIII, multi-hit, ETOF Upgrade, MRPC, time resolution

PACS: 29.40.Cs, 29.40.Mc **DOI:** 10.1088/1674-1137/37/9/096002

1 Introduction

BESIII [1] is a modern spectrometer located at the upgraded Beijing Electron Positron Collider (BEPC II), which runs in the energy region 2–4.6 GeV and aims at τ-charm physics [2]. Particle identification (PID) plays an essential role in the experimental study. One of the main sub-detectors, the time-of-flight (TOF) system, responding for trigger and PID, consists of a barrel and two endcaps. Its capability of PID is determined by the flight time difference of particles species and the time resolution of the detector. The current TOF system based on plastic scintillation and photo-multiplier (PM) was built in 2001 [3–5]. The calibration result of the endcap TOF system shows that the time resolution for electrons in BhaBha events is 148 ps, which is significantly worse than the resolution for mouns in dimu events (110 ps, the designed goal). It's also found that scattering in main drift chamber (MDC) endplate materials can significantly influence the measured times of electrons in BhaBha events [6]. These findings indicate that the contribution to timing performance from multiple scattering interaction in the endcap material between the MDC and the endcap time-of-flight (ETOF) is important. Improvement is needed for the ETOF system to better meet the BESIII physics goals. The R&D for this upgrade began in 2010. Monte-Carlo (MC) simulation serves as an important tool to guide the upgrade, by comparing the performances of TOFs based on different technologies and optimizing the prototype design. In this paper a detailed simulation study, including all main features of the BESIII ETOF system, is performed. The GEANT4 [7, 8] package (GEANT version 4.09.02.p01), commonly used in high energy experimental physics, is taken as the simulation tool.

2 Endcap detector's configuration of BESIII

The BESIII ETOF system is located between a helium-based multilayer MDC and an CsI(Tl) crystal electromagnetic calorimeter (EMC) inside the BESIII spectrometer. The cross-sectional view of the ETOF system is shown in Fig. 1. Please note, although not shown in the figure, there are some materials, such as cables and readout electronics equipment, located between the endplate of the MDC endcap and the ETOF.

Received 12 November 2012, Revised 9 April 2013
* Supported by National Natural Science Foundation of China (10979003)
1) E-mail: swing@ustc.edu.cn
2) E-mail: licheng@ustc.edu.cn

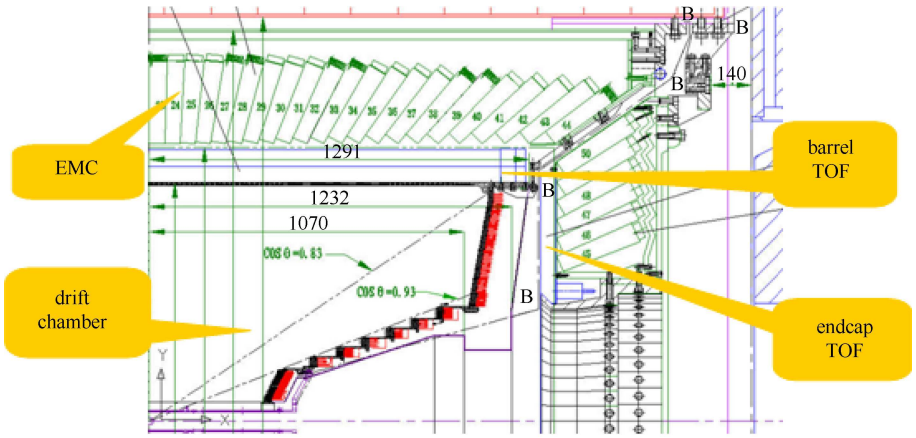

Fig. 1. Schematic drawing of the TOF in BESIII.

Because the description of the detector structure and materials in the full BESIII MC framework is quite complicated and difficult to modify and tune, we develop a simplified model to do this job for the ETOF system. The main structure in our simulation is shown in Fig. 2. Basically it consists of three parts. The left part is the MDC volume, filled with a gas mixture of 60% He and 40% C_3H_8. The field and sensitive wires in the MDC are not simulated, since their contribution to multiple scattering is small.

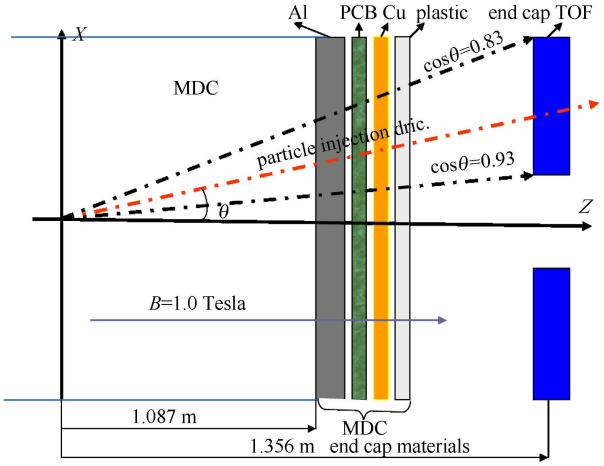

Fig. 2. Detector layout in simulation.

The middle part, including the endplate of MDC and the readout electronics and cables, contains the major material budget between the MDC and ETOF. The composition and equivalent thickness of the materials in this part are estimated by using the full BESIII MC framework. Virtual (non-interacting) particles are emitted toward the MDC endcap region with $0.83 \leqslant \cos\theta \leqslant 0.93$ (θ is the polar angle as shown in Fig. 2). For each step the virtual particle travelled, the material composition and equivalent thickness (along Z direction) are recorded and accumulated until the virtual particle hit the ETOF. We find four major media dominate the material budget, namely aluminum, printed circuit board (PCB), copper and plastic. Their equivalent thicknesses are 21.12 mm, 9.77 mm, 0.58 mm and 9.59 mm, respectively.

The right part is the ETOF system, in which the detailed structure depends on the detector technology used and will be addressed in the following part of the paper. It's worth noting that although there are further materials near the ETOF modules (such as the gas box, the glass and the FEE, etc.), our simulation results show that their impact on ETOF performance is found to be negligible. The magnetic field of BESIII is a uniform field of 1 T along the Z direction.

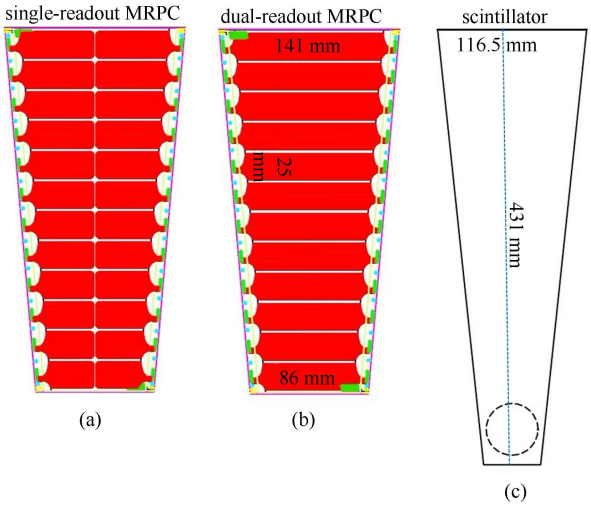

Fig. 3. Structure of BESIII ETOF module. For (c) the current scintillator-based ETOF module and (a) the single-readout MRPC-based ETOF module and (b) the dual-readout MRPC-based ETOF module.

The current TOF endcap, each consisting of 48 trapezoidal-shaped plastic scintillation (Bicron 404)

modules, is located at 1330 mm away from the interaction point (IP) along the beam direction (Z axis in the global BESIII coordinate system, as in Fig. 2). For each scintillator module, the length is 431 mm and the thickness is 48 mm, covering an azimuthal angle range of 7.5°, as shown in Fig. 3(c). More details can be found in Ref. [9].

3 Simulation results of scintillator-based ETOF and discussion

To simulate the BhaBha events, which play an important role in the offline calibration of BESIII TOF system, electrons with momentum of 1.5 GeV/c are emitted from the IP (all the simulation results in this paper are from Bhabha events, if not otherwise explained). The injection direction with respect to the Z axis is chosen to be $\cos\theta = 0.9$ so that the extrapolated hit point is located near the center of the ETOF module in the radial direction. In the simulation we use standard GEANT4 electromagnetic (EM) physics process including ionization, multiple scattering, bremsstrahlung and the gamma interaction with default settings for production thresholds of secondary particles.

Particles hitting the ETOF are electrons, positrons and gammas. The hit position distributions on ETOF module, of primary electron (ie. Bhabha electron), secondary electron/positron and gamma, are shown in Fig. 4(a), (b) and (c) respectively. The ETOF module boundaries are also shown in the figures. In order to test the worst case, the extrapolated hit points are chosen to be at the center of an ETOF module (so the hit multiplicity is the highest).

To further understand the feature of the secondary charged particles and the effect on ETOF timing, we show in Fig. 5 the radial hit position distribution on ETOF of the secondary electron and positron, as a function of transverse momentum (P_t). Two notable bands can be seen in the figure, one with higher P_t and R close to 64 cm, while another with very low P_t and R close to 54 cm. Combined with Fig. 4(b), we can conclude a rough scenario that the band near R=64 cm mainly comes from primary electrons and bremsstrahlung gamma (converting to electron/position pair), mostly following the direction of primary electrons, while another band located at R=54 cm are those low energy (thus also low P_t) electrons and positrons generated from the EM shower or from energetic ionization in the MDC endplate material. In strong magnetic field these low energy electrons or positrons basically travel along the field line, thus their hit position on ETOF reflects the position where they are generated, which is R∼54 cm from Fig. 2 (∼1.1 m ×tanθ).

For each primary electron, a large number of secondary electron, positron and gamma are produced in MDC endcap region causing multi-hit on a scintillator module. More quantitatively, we define the multi-hit rate as the fraction of events with 2 or more hits on one ETOF readout cell. We find the multi-hit rate of scintillator-based ETOF is about 71.5%. Multi-hit can badly influence the timing performance of ETOF by distorting the output signal shape and amplitude that are hard to calibrate offline. Note there is no tracking information available for these secondary particles in the calibration.

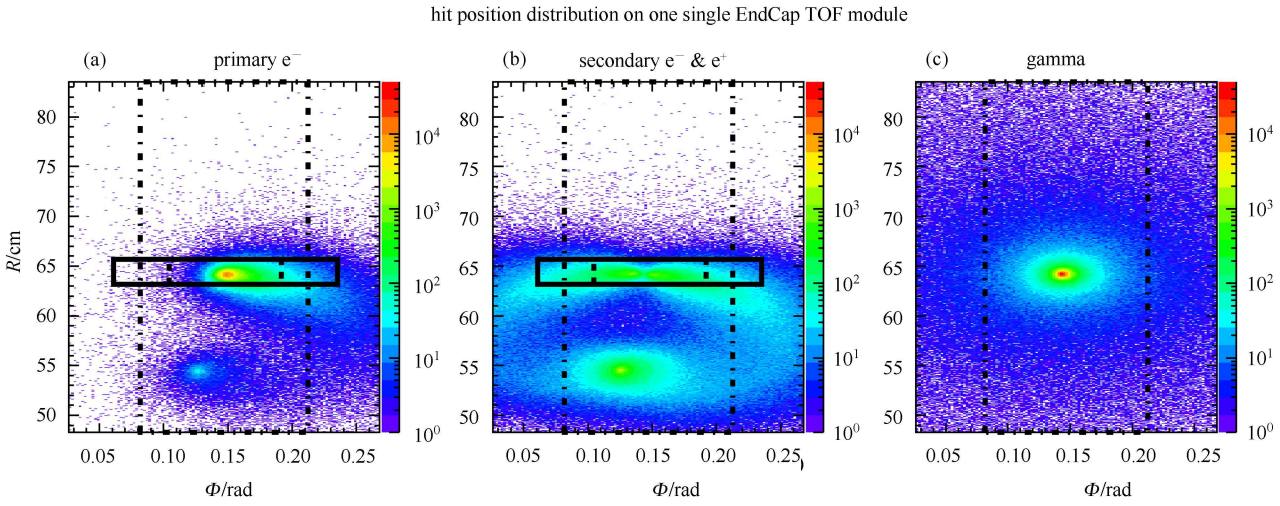

Fig. 4. Hit position distribution detected by ETOF. The large rectangle in the dashed line shows the boundary of one scintillator-based ETOF module, while the two smaller rectangles in the solid/dashed line denote the readout-pad boundaries of dual/single readout MRPC module.

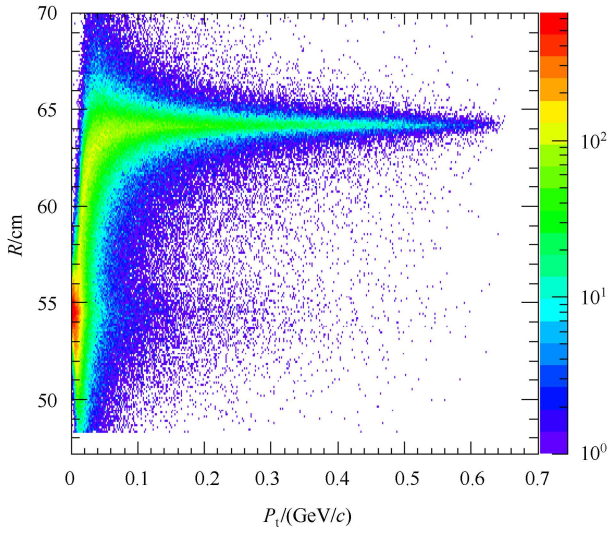

Fig. 5. The relationship of R with $P_{\rm t}$ of secondary charged particles.

To study the effect of the complex hit position distribution structure and the high multi-hit rate on ETOF timing, we make a semi-quantitative calculation by evaluating the hit time and position information. For each track, the measured arrival time is the sum of particle flight time from the IP all the way to ETOF and the signal's transmission time to the readout end. We assume a simple one-dimensional linear timing dependence on the hit position. In the scintillator, the signal transmission time can be expressed as $(R-R_0)/v$, where R_0 is the radial position of the PM, and v is the effective transmission velocity in scintillator. R_0 is 47.2 cm in the current BESIII ETOF design and v^{-1} is measured to be 80 ps/cm [6]. In each event, the earliest arrival time at the PM among all hits is taken as the measured TOF. The TOF distribution is shown in Fig. 6. Beside the nominal TOF peak at around 6.2–6.4 ns caused by primary electrons, another peak with much smaller TOF around 5.5 ns is clearly visible in Fig. 6. The left peak is about 0.9 ns earlier in time than the nominal peak - this is understood as a consequence of secondary electron/positron band at low energy and low R in Fig. 5. In Fig. 5, the difference in R for the two main bands is 10 cm. Consider the transmission velocity of fluorescent photons in the scintillator, their arrival time difference will be 0.8 ns, agreeing well with Fig. 6. The difference in flight time from the IP to ETOF is relatively small, since electron or positron travels at a velocity very near to the speed of light. Our simulation also confirms this point. We also simulated the time distribution of a muon (p=1.5 GeV/c) that hits ETOF, also shown in Fig. 6. It's clear that the peak near 5.5 ns of muons is significantly reduced compared to the electron case, indicating the much reduced multi-scattering effect by materials at the MDC endplate. A similar feature was observed with the full BESIII MC framework (including fluorescent photon generation and transmission), as well as the calibration results with experimental BhaBha and dimu data collected by BESIII [6]. The consistency of these results validates the reliability of our simulation.

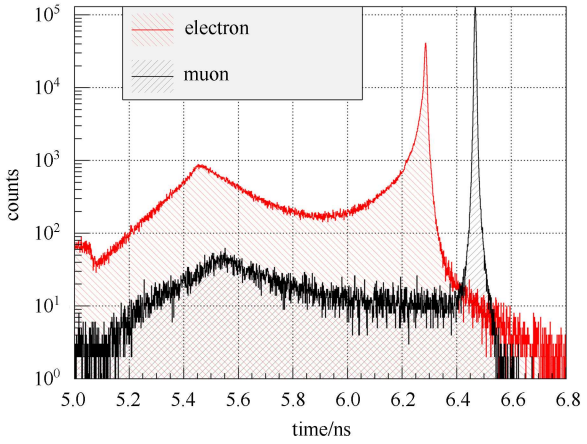

Fig. 6. The timing distribution of scintillator-based ETOF.

The simulation results of scintillator-based ETOF show that the multiple scattering effects, mainly from the MDC endcap materials, can cause multi-hit on the ETOF's readout cell and make the hit position distribution structure on the ETOF's readout cell complex by producing secondary particles in the materials and significantly influence the performance of ETOF. Furthermore, the complex hit position distributions also indicate that the tracking accuracy is also worse in the endcap region than that in the barrel region, which consequently makes the position-dependent time calibration difficult.

To reduce the multi-hit probability and simplify the hit position distribution structure, smaller readout cell size is favored. However, reducing module size means increasing readout channels, which is not suitable for scintillator-based ETOF since the PM dedicated in strong magnetic field is rather expensive. The MRPC, first developed by LHC-ALICE TOF collaboration [10], is a new type gaseous detector with good time resolution and high detection efficiency. Furthermore, it can be designed with a smaller readout cell structure and the cost of each readout cell is much lower. It is considered a suitable candidate for the upgrade of BESIII ETOF system.

The R&D for such an upgrade began in 2010. In each endcap there are 36 trapezium-shaped MRPC modules. Fig. 7 shows the top and side view of an MRPC module appropriate for BESIII. It has a double-stack structure with twelve gaps. Floating glass sheets are used as the resistive plates. The thicknesses are 0.4 mm and 0.55 mm for the inner and outer glass, respectively. The gap between the glass is 0.22 mm. The thickness of the

honeycombs, readout pads, PCB and Mylar boards are also shown in Fig. 7. The MRPC is placed in an aluminum box with a thickness of 1 mm which is filled with a standard gas mixture for MRPC. The composition of the gas is 90% Freon +5% SF6+5% C4H10 [11].

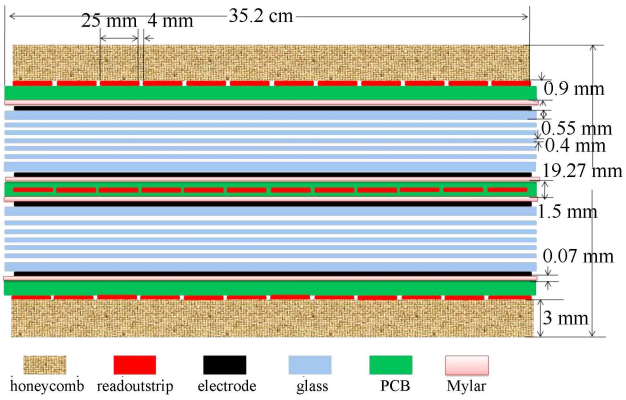

Fig. 7. Side view of an MRPC module for BESIII ETOF upgrade.

Two types of MRPC modules with different readout pad structure are designed for the upgrade. The dual-readout MRPC module has 12 readout pads, each 2.5 mm wide, with length ranging from 8.6 cm to 14.1 cm. Signals are readout at both ends of the pad. The single readout MRPC module has a similar structure except that each readout pad is divided into two from the center (see Fig. 3). In order to study the improvement with this upgrade, the scintillator-based ETOF system is replaced with the proposed MRPC based ETOF system in the simulation setup shown at Fig. 2.

4 Simulation results of MRPC based ETOF and comparison

The hit position distributions on MRPC based ETOF module, of primary electron, secondary electron/positron are shown in Fig. 4(a) and (b) respectively. The module boundaries are also shown in the figures like that of the scintillator-based ETOF case. Note in Fig. 4(c) the MRPC pad boundaries are not shown since MRPC are intrinsic not sensitive to gamma (usual efficiency <0.1%).

It's found that the multi-hit rate (per readout channel) is 21.8% or 16.7% for MRPC ETOF with dual-readout or single-readout module design, dropping significantly from scintillator-based ETOF's 71.5%. Note the readout cell of MRPC based ETOF is much smaller than that of scintillator-based ETOF and all three components in Fig. 4 (primary electron, secondary electron/position and gamma) contribute for a scintillator while gamma hits are not accounted for MRPC.

With a significantly reduced multi-hit event rate and simpler hit position distribution structure, one can expect better timing performance and easier calibration for an MRPC-based ETOF rather than a scintillator-based ETOF. To compare the timing performance of both types of ETOF, we also make a semi-quantitative calculation for an MRPC-based ETOF in a similar way as the scintillator.

On the MRPC readout pad, electric pulses propagate to the FEE-fed end. For each track, the signal transmission time on the readout pad is calculated as L/v, where L is the distance between the hit and the feed-out end, and v is the propagation velocity of the electric pulse.

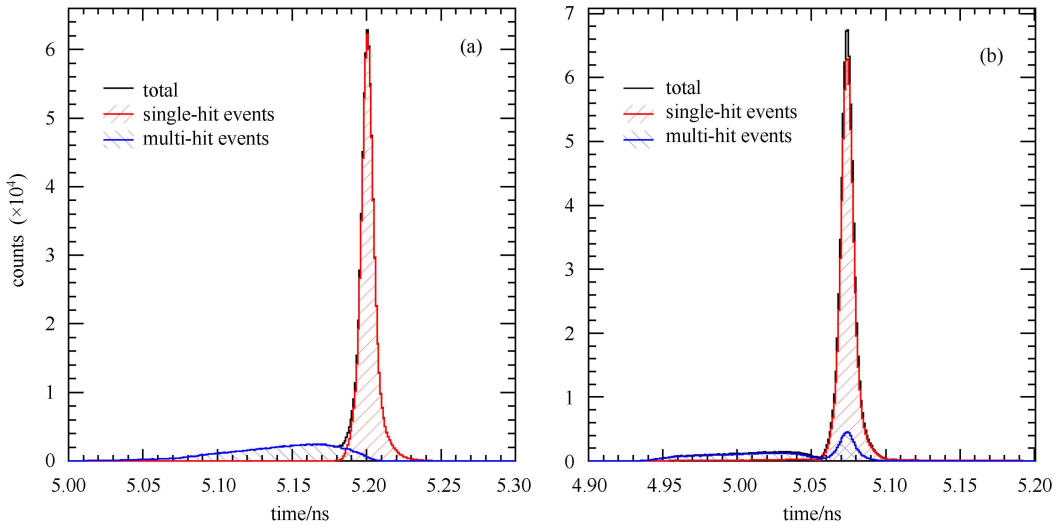

Fig. 8. The timing distribution of MRPC-based ETOF, for (left) the dual-readout MRPC design and (right) the single-readout MRPC design. (a) Dual-readout MRPC; (b) single-readout MRPC.

Table 1. Time difference for scintillator and MRPC based ETOF.

types	$\Delta t \geqslant 30$ps	$\Delta t \geqslant 50$ps	$\Delta t \geqslant 80$ps	$\Delta t \geqslant 100$ps	$\Delta t \geqslant 150$ps
scintillator	40.0%	36.2%	33.3%	32.1%	30.0%
dual-readout MRPC	16.3%	11.6%	5.9%	3.3%	0.5%
single-readout MRPC	9.4%	7.1%	3.7%	1.9%	0.0%

For MRPC modules used in BESIII ETOF, v^{-1} is measured to be 45 ps/cm [12, 13], nearly twice as fast as that in an ETOF scintillator. Also in each event, only the earliest signal arrival time is taken as the measured TOF. For single-readout MRPC the signal is chosen to be feed-out from the left end, while for dual-readout MRPC, the time measured is chosen as the average measurement from both sides. The TOF distribution of an MRPC ETOF is shown in Fig. 8. It's obvious that the false timing from secondary particles is greatly suppressed compared to the scintillator ETOF case.

We make a comparison of timing performance from all three kinds of ETOF design (two detector technology, and two readout pad designs for MRPC) and show the result in Fig. 9. Again we see clear improvement with MRPC-based ETOF. For the two kinds of MRPC readout design, the single-readout method has better timing property due to less multi-hit rate compared to the dual-readout one. However, one should know for single-readout MRPC, the timing is hit position dependent thus requiring precise tracking which is not easy at BESIII endcap region. Dual-readout MRPC basically does not need very good tracking since the hit position uncertainty cancels out in time averaging from both ends. Further investigation needs more detailed simulation and experimental efforts and is beyond the scope of this paper.

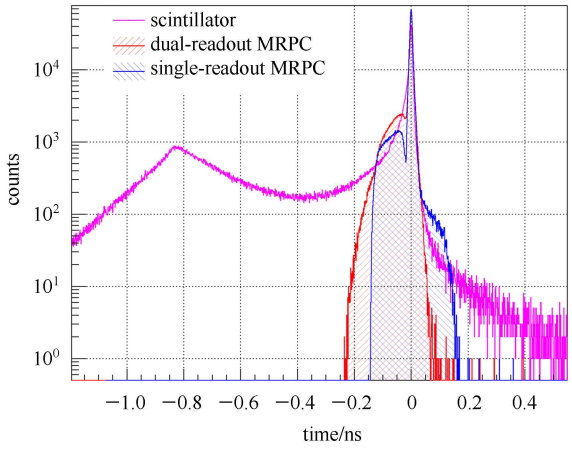

Fig. 9. Comparison of timing of scintillator-based and MRPC-based ETOF. (Peaks are moved to zero ns).

To further quantify the difference in timing for the three kinds of ETOF design, we calculated the fraction of events in which the time difference (with respect to time=0 in Fig. 9) was larger than 30 ps, 50 ps, 80 ps, 100 ps and 150 ps. The results are shown in Table 1. We can clearly see that the upgrade can further reduce the adverse influence of the multi-hit on the timing of ETOF.

5 Conclusion

We have developed a GEANT4-based MC model to study the timing property of the two types of ETOF design, based on scintillator or MRPC. The simulation results show that the multiple scattering process in the material budget between MDC endcap and ETOF will produce a large number of secondary particles that will affect the timing of the plastic scintillator used in the current BESIII ETOF system, causing a high multi-hit rate per readout channel (71.5%) and a double-peak structure in the TOF spectrum for BhaBha events. The timing peak with TOF abnormally small is contributed by the secondary particles with very low energy and is about 0.9 ns earlier to the nominal timing peak. These results are consistent with the offline calibration results with experimental BhaBha data. The multi-hit rate per readout channel of MRPC is much lower (21.8% for dual-readout MRPC and 16.7% for single-readout MRPC design), and the timing performance of MRPC is also better.

References

1 Ablikim M et al. Nucl. Instrum. Methods A, 2010, **614**: 345
2 Asner D et al. Int. J. Mod. Phys. A, 2009, **24**: Suppl. 1
3 LI X et al. High Energy Physics and Nuclear Physics, 2005, **29**: 586 (in Chinese)
4 TANG Ze-Bo et al. High Energy Physics and Nuclear Physics, 2006, **30**: 445 (in Chinese)
5 AN Shao-Hui et al. High Energy Physics and Nuclear Physics, 2005, **29**(1): 775 (in chinese)
6 ZHAO Chuan et al. Chinese Physics C (HEP & NP), 2011, **35**: 72
7 Agostinelli S et al. Nucl. Instrum. Methods A, 2003, **506**: 250
8 Allison J et al. IEEE Trans. Nucl. Science, 2006, **53**: 270
9 LIU Y et al. Nucl. Instrum. Methods A, 2011, **629**: 87
10 http://alice.web.cern.ch/Alice/TDR/alice-tof.ps
11 SUN Yong-Jie et al. Chinese Physics C (HEP & NP), 2012, **35**(5): 429
12 Akindinov A et al. Nucl. Instrum. Methods A, 2004, **532**: 611
13 WU J et al. Nucl. Instrum. Methods A, 2005, **492**: 344